Photodissociation and charge transfer photodynamics in crystalline krypton doped with F_2 and Xe

H. Kunttu,[a] E. Sekreta, and V. A. Apkarian[b]
Department of Chemistry, Institute for Surface and Interface Science, University of California, Irvine, Irvine, California 92717

(Received 4 February 1991; accepted 1 March 1991)

Long-range migration of F atoms upon photodissociation of F_2 is demonstrated in mixed F_2:Xe:Kr solids by monitoring arrival of F atoms at Xe sites. The impulsive migration probabilities are wavelength dependent. At excess energies above 2.4 eV migration lengths spanning 15 lattice sites are observed. Migration is not observed for excess energies below 1.9 eV. The photodynamics of charge transfer states in F:Xe:Kr solids is presented. Both diatomic Xe^+F^-, and mixed triatomic $(KrXe)^+F^-$ exciplexes are observed. The XeF(C) and $(KrXe)^+F^-$ states are strongly coupled and decay radiatively with a lifetime of 80 ns. These states are populated via excited vibrations of XeF(B) and XeF(D). A crossing between XeF(D) and KrXeF potentials is identified. Above this crossing the lower manifold of charge transfer states are directly populated, while a delay of 10 ns is observed below the crossing. XeF(B, $v = 0$) remains uncoupled from the rest of charge transfer states. Implications with respect to solid state exciplex lasers are discussed.

I. INTRODUCTION

Halogen-doped rare gas solids (X/RGS) provide convenient systems for probing a wide variety of photodynamical phenomena in condensed phases. The well characterized nature of Rg–Rg′ and Rg–X pair interactions both in the ground and excited states, combined with the detailed knowledge of the static and dynamic properties of rare gas solids, makes X/RGS a simple model system in which rigorous tests of many-body dynamics can be made. The existence of luminescent charge transfer transitions in X/RGS makes these systems particularly attractive from an experimental point of view, since the sensitive technique of laser induced fluorescence can be applied to follow the dynamics of atomic fragments. In addition to serving as prototypes of condensed phase molecular dynamics, there are practical motivations guiding these investigations. The development of solid state exciplex lasers,[1-3] and optical energy storage[4] are two such examples. A detailed understanding of charge transfer energetics and dynamics is a prerequisite for such developments. In this paper we report on photodynamics in a solid Kr host doubly doped with Xe and F_2. The main aims of the study are twofold: to probe the long-range migration of F atoms upon photodissociation of F_2, and characterization of charge transfer states and associated photodynamics in F/Xe/Kr crystals.

Due to the simplicity of its electronic states,[5] fluorine represents a rather ideal diatomic for photodissociation studies in RGS. As such, it has been studied theoretically by molecular dynamics simulations,[6] and several experimental studies probing different aspects of the dynamics have already been reported.[7-9] Upon optical access of the repulsive $^1\Pi_u$ potential, wavelength dependent quantum yields of dissociation in solid Ar[8] and Kr[9] have been reported. The cage exit probabilities in these systems reach unit quantum yield at excess energies above 2.5 eV, in agreement with the theoretical simulations. Temperature dependence studies in Kr have shown a strong effect for molecule–lattice prealignment on cage exit probabilities, as predicted by theory.[9] Dissociation of diatomics in rare gas solids is determined by the cage exit probabilities of impulsively generated atoms. In the case of F atoms, the exit occurs through well defined windows of the lattice and the fragments maintain most of their initial kinetic energy. One of the fascinating consequences of this process is that after cage exit, F atoms undergo long-range migration along face diagonals of the solid.[6] Until the present, this theoretical prediction had not been verified experimentally, although long-range migration of F atoms had been demonstrated in the analogous process of radiative dissociation of rare gas fluoride exciplexes.[7,8] In a solid Kr host, doped simultaneously with Xe and F_2, it is possible to probe long-range migration of F atoms by monitoring their arrival at Xe sites. In the present paper we report such studies, and show that long-range migration probabilities are strongly dependent on initial energy of the fragments.

A variety of charge transfer states have been discovered in halogen doped rare gas solids. In Cl, Br, and I doped solid Xe,[10] and in Cl doped Kr,[11] optical excitation leads to delocalized charge transfer states which can be described as a Rydberg progression of holes.[12] These states relax rapidly to the triatomic Rg_2X configuration and subsequently decay radiatively. In F doped Kr, the Rydberg–hole progression collapses, limiting the delocalization of the positive charge to the immediate neighbors of the halogen ion.[7] As in the case of Xe, for all the halogen atoms doped in solid Kr as well, emission from the triatomic Kr_2X molecular exciplex is observed.[13] In F doped Xe,[10] and also in F:Kr doped Ar,[7] the excitation spectra reveal the diatomic XeF and KrF resonances, however, emission is only observed from the triato-

[a] Present address: Department of Physical Chemistry, University of Helsinki, SF-00170, Helsinki, Finland.
[b] Alfred P. Sloan Fellow.

mics—from the mixed triatomic ArKrF exciplex in the latter case. The interconversion from diatomic to triatomic configurations is fast, estimated to proceed on a time scale shorter than 500 fs. In such ternary solids as F/Xe/Ar and F/Xe/Ne, the diatomic XeF exciplexes maintain their integrity in both excitation and emission spectra.[14,15] However, as will be discussed, in F/Xe/Kr, both diatomic Xe^+F^- and mixed triatomic $(KrXe)^+F^-$ charge transfer states coexist. This is not a unique situation. In studies of Cl/Xe/Ar in the liquid phase the coexistence of XeCl and ArXeCl states were noted,[16] and in more recent studies, XeCl and NeXeCl states were simultaneously observed in emission in solid Ne.[17] The subtle equilibrium between these molecular charge transfer states, which is discussed in this paper, has not been previously studied in any detail. This dynamics has serious bearings with respect to laser action in these media. To date, laser action has been demonstrated over the $D \rightarrow X$, $B \rightarrow X$, and $C \rightarrow A$ transitions of XeF in solid Ar,[1,2] and the $D \rightarrow X$ transition of XeF in solid Kr[3]—systems in which the diatomic exciplexes maintain their integrity. The failure of observing laser action in triatomic solid state exciplexes is ascribed to an intense reabsorption by the exciplex.[6,7,13] However, little is known about the upper states responsible for this reabsorption in condensed media. In F:Xe:Kr solids, we discover that this reabsorption leads to emission from the D state, and as such should be useful in revealing the photodynamics of highly excited charge transfer states. Finally, the rather mundane question, as to which diatomic exciplex may be possible to isolate in a given host is discussed.

II. EXPERIMENTAL

The experiments were conducted in free standing crystals of krypton of $\sim 1\ cm^3$ volume. The crystal growth methodologies are those developed by Schwentner and coworkers[18] with minor modifications. The crystals are grown in a rectangular Pyrex cuvet of 1 cm $\times$ 1 cm cross section, fused to a 1/4 in. glass tube. The tube is fed through a double "O"-ring connection on the cryostat vacuum shroud. The Pyrex mold is initially brought into contact with the cryotip (Air Products Displex, DE-202), and the premixed gas is deposited at a backing pressure of ~ 200 Torr. After a sufficiently long crystal is formed, the mold is manually retracted. The cryotip consists of an OFHC-copper block, in which a rectangular hole is cut to anchor the crystal. Temperature is measured with a gold-chromel thermocouple embedded in the crystal during its growth. The solids prepared with this method are polycrystals of high optical quality. Scattering losses inside the crystal are typically a few per cent, for a pathlength of $\sim$ 1cm in the near-uv spectral region.

The poor thermal conductivity of the Pyrex mold and the RGS combine to yield a large thermal gradient across which the crystal grows. The temperature in the center of the crystal during deposition is typically 30–45 K. Under these conditions, clustering of dopants, or segregation of guest and host, are expected phenomena. In the case of F_2-doped solid Ar and Kr for dilution in excess of 1:3000, no evidence for concentration gradients or of clustering has been observed. This assessment is based on qualitative observations, such as the uniformity of emission or scattering in the irradiated volume of the crystal as inspected by eye, and also on more quantitative, however, less direct observations, such as photodissociation kinetics. In studies of F_2 photodissociation, an induction period in the exciplex emission growth was related to nonuniform distribution of dopants, which corresponded to only few per cent of the total F_2 concentration.[8] The statistical nature of isolation is verified in the present system, as will be discussed below. However, we mention that in other guest/host combinations extensive clustering is observed in solids grown by these methods.

Multigas excimer lasers or excimer pumped dye lasers equipped with doubling crystals were used as excitation sources. The duration of the doubled dye laser pulse was measured to be 7 ns. Emission spectra were recorded with an optical multichannel analyzer fitted with a gated intensified diode array (EG&G OMA III). A mercury penlight is used for spectral calibration of the OMA. Growth dynamics of different emission bands was monitored with a photomultiplier tube (PMT), and a boxcar integrator after dispersing the emission with a 1/4 m monochromator. Radiative lifetimes were measured with a PMT or a fast PIN photodiode having a rise time of 2 ns. The signals were recorded and averaged with a 500 MHz digital oscilloscope (Tektronix 2440).

Excitation spectra were recorded using the monochromatized output of a 150 W Xe arc lamp. Prior to recording the spectra, F_2 was dissociated with broadband output of the lamp. Several hours of irradiation was needed to produce sufficient concentration of atomic fluorine for spectroscopic investigations. The excitation and detection arms of the spectrometer were equipped with 0.3 m monochromators (McPherson 282). A PMT of flat spectral response in the 200–900 nm range (Hamamatsu RG-666) was used to detect the fluorescence. In most of the experiments the monochromator slits were adjusted to a ~ 2 nm bandpass. The search for vibrational structure in the spectra was conducted with a 0.3 nm bandpass. The excitation source was chopped at ~ 1 kHz and the signal was detected with a lock-in amplifier (SRS, SR-510). Background corrected spectra were obtained after division with the spectral profile of the source, recorded under identical conditions.

High purity gases without further purification were used. The manufacturers specifications were: F_2 (97%), Kr(99.999%), Xe (99.999%). Gas samples were manipulated in either a greaseless, glass vacuum line, fitted with Teflon seated stopcocks, or in a Monel vacuum manifold.

III. RESULTS

A. Photodissociation of F_2

Photodissociation of F_2 can be accomplished in rare gas solids via two distinct mechanisms: (a) direct dissociation via the $^1\Pi_u$ absorption continuum of F_2, or (b) two-photon induced harpooning.[7-9] Either of these mechanisms lead to efficient and permanent generation of atomic fluorine when carried out at cryogenic temperatures near 10 K. In the present, we concentrate on mechanism (a). Two-photon processes are eliminated by carrying out the studies at low laser fluence. The photogeneration of F atoms is followed by mon-

itoring emission from a particular rare gas–fluoride exciplex. In F_2:Xe:Kr ternary solids, this can be accomplished by excitation of either Xe^+F^- or Kr^+F^- charge transfer states. As a result, in addition to photodissociation kinetics, information is obtained about the spatial distribution of atoms. A minimal knowledge of the spectroscopy of charge transfer states in this system is necessary for the understanding of the results to be reported in this section. A relatively sharp resonance, with a threshold near 280 nm, is observed for the excitation of charge transfer states in solid Kr doped with atomic fluorine. Excitation above this threshold leads exclusively to emission from $Kr_2^+F^-$, which peaks at 453 nm.[7] The charge transfer states of XeF in solid Kr can be accessed in a wide spectral range, the threshold being ~390 nm. Depending on the excitation wavelength, the possible emissions are the diatomic $D\rightarrow X$ (303 nm), $D\rightarrow A$ (364 nm), $B\rightarrow X$ (428 nm), and $C\rightarrow A$ (575 nm) transitions. Thus at excitation wavelengths longer than 280 nm, only those F atoms which are nearest neighbors to Xe are monitored. At shorter excitation wavelengths, all F atoms in the solid can be monitored simultaneously.

Figure 1(a) shows a typical emission spectrum obtained with 275 nm excitation of a solid of original composition F_2:Xe:Kr of 1:1:3000. The spectrum was recorded after completion of growth of the observed emissions. At this wavelength, all of the observed emissions in the spectrum grow exponentially with irradiation time. The broad $Kr_2^+F^-$ emission band centered at 450 nm is a direct measure of F atoms trapped in the bulk of Kr, and the XeF emissions at 303 and 364 nm indicate that a significant fraction of F atoms reach Xe atoms. The strong $Kr_2^+F^-$ emission overlaps the expected XeF $B\rightarrow X$ and $C\rightarrow A$ emissions. The excitation wavelength in this case matches with both KrF($B\leftarrow X$) and XeF ($D\leftarrow X$) resonances; therefore, the probe sensitivity for the two transitions is comparable.

When the temperature of the solid is raised above 20 K, the XeF emissions gain intensity while the emission near 450 nm is drastically reduced, as illustrated in Fig. 1(b). In fact, the $Kr_2^+F^-$ emission which dominates in trace (a) of Fig. 1, is completely absent in trace (b). Instead, a new emission band at 465 nm is observed. This emission is assigned to the mixed triatomic, $(KrXe)^+F^-$, exciplex. Beside the spectral shift, this emission can be distinguished from that of $Kr_2^+F^-$ by its narrower spectral width and shorter fluorescence lifetime (80 ns vs 140 ns for $Kr_2^+F^-$). The observed strong temperature effect can clearly be ascribed to thermal diffusion of F atoms and subsequent trapping next to Xe. The thermal onset of the spectral transformation is 15 K, somewhat lower than the diffusion temperature of F atoms in pure solid Kr, which is observed to be ~18 K.[8] Thus it can be concluded that Xe acts as a deep trap, and therefore as an efficient scavenger for mobile F atoms in solid Kr. This result is not too surprising given the fact that the XeF(X) potential is nearly an order of magnitude deeper than that of KrF(X).[19,20]

Similar studies were conducted at 308, 351, and 360 nm. The 308 nm results were qualitatively similar to those at 275 nm, namely, an exponential growth in the XeF emission intensity is observed, and upon warmup, this emission intensifies by nearly fivefold. The exponential growth rates at both 308 and 275 nm yield quantum yields near unity for the dissociation of F_2, in agreement with the measurements in pure Kr.[9] A very different behavior is observed when dissociation and probing are carried out at longer wavelengths. Spectra are shown in Fig. 2 which are taken from a study using a dye laser at 360 nm as both dissociation and probe source. At this wavelength, while F_2 readily dissociates, only XeF ($B/C\leftarrow X$) resonances are accessible. After extensive irradiation of the solid at 10 K, only a very weak emission is observed (see Fig. 2). Upon warmup of the solid, without further irradiation, the XeF $B\rightarrow X$, $C\rightarrow A$, and $(KrXe)^+F^-$ emissions become clearly visible. (The sharp $B\rightarrow X$ emission appears as a shoulder on the broad KrXeF emission band.)

In Fig. 3, the evolution of $(KrXe)^+F^-$ emission intensity as a function of exposure to laser pulses at 351 nm is shown. A very weak emission is observed immediately after exposure to the laser; and at 12 K the emission intensity remains essentially constant after ~1000 pulses. At this

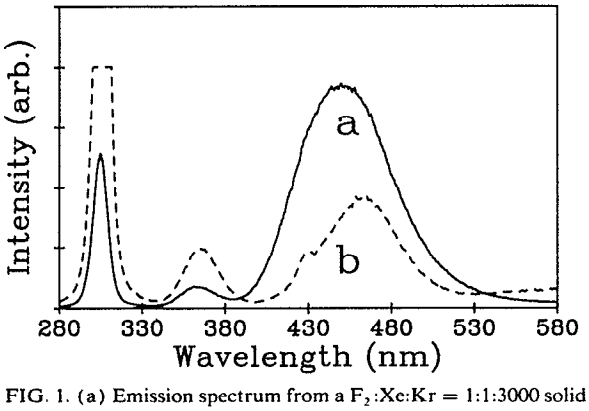

FIG. 1. (a) Emission spectrum from a F_2:Xe:Kr = 1:1:3000 solid at 12 K. Spectrum was recorded with an optical multichannel analyzer (OMA III) after extensive irradiation with 275 nm laser (also used as an excitation source). The observed emission bands are: 303 nm: XeF ($D\rightarrow X$); 364 nm: XeF ($D\rightarrow A$); and 453 nm: Kr_2 ' F . (b) The same spectrum at 19 K. The observed new emissions are: 465 nm: (KrXe) ' F and 428 nm (shoulder): XeF($B\rightarrow X$).

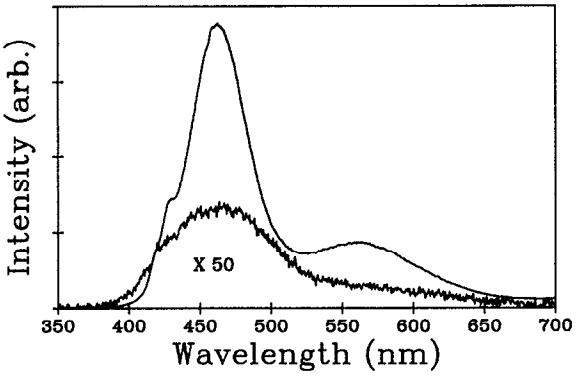

FIG. 2. Emission spectra from a F_2:Xe:Kr = 1:1:3000 crystal with 360 nm excitation. Spectra were obtained after extensive irradiation at 360 nm. Lower trace: T = 10 K: upper trace: T = 15 K. Note the different sensitivity scale in the low temperature spectrum. For band assignment, see Fig. 1.

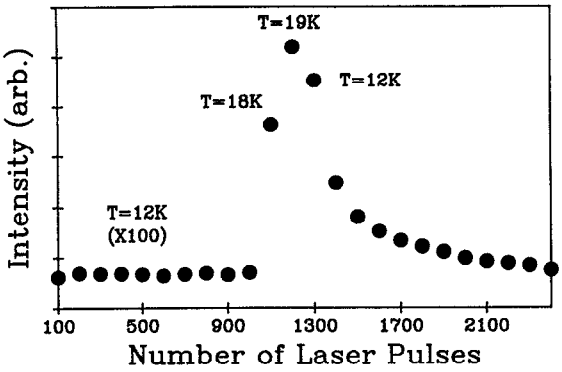

FIG. 3. $(KrXe)^+F^-$ emission intensity as a function of irradiation time with 351 nm laser (346 mJ cm^{-2}, 10 Hz repetition rate). Each data point corresponds to accumulation of 100 excitation pulses with OMA. The original sample composition is F_2:Xe:Kr = 1:1:7000.

wavelength, the photodissociation quantum yield of F_2 in Kr is 0.75.[9] Therefore, at the excitation intensity of 6.1×10^{17} photons cm^{-2} $pulse^{-1}$, the F atom growth lifetime corresponds to 300 laser pulses (using the gas phase absorption cross section of F_2:0.7×10^{-20} at 351 nm[5]). Upon raising the temperature of the crystal to 19 K, nearly 500-fold increase in the emission intensity is observed. Thus in contrast to the studies at shorter wavelengths, a negligible fraction of the F atoms are produced next to Xe in the photodissociation process at 12 K. In this case, Xe–F pairs are formed exclusively by the thermal diffusion of F atoms subsequent to their photogeneration.

As illustrated in Fig. 3, the KrXeF emission reaches a maximum with irradiation time. Further irradiation causes a decay in both KrXeF and XeF ($C\rightarrow A$) emissions. It was verified that at temperatures above 20 K, when the sample is left in the dark the XeF emission intensity recovers at least partially. There are two obvious mechanisms for the reduction of Xe–F emission, (a) formation of XeF_2, which would constitute a permanent loss channel since it does not absorb 351 nm radiation, (b) radiative dissociation of exciplexes which leads to ejection of F atoms out of the trap site. The latter mechanism has previously been characterized in several studies.[7,8] In effect, since several of the radiative transitions involve repulsive ground states, e.g., KrXeF and XeF($C\rightarrow A$), F atoms with sufficient kinetic energy are created to exit the solid cage. The observation of signal recovery in the dark would indicate that the F atoms are available to diffuse back to the Xe sites, presumably from temporary trapping sites composed strictly of Kr nearest neighbors. Photomobility of F atoms due to radiative dissociation of exciplexes would imply that at wavelengths where both dissociation of F_2 and excitation of exciplexes is possible, only a photochemical steady state between F and F_2 can be established. The suspected presence of XeF_2 further complicates this situation, such that in concentrated solids, it is difficult to establish the exact number density of F atoms.

TABLE I. Emission characteristics of F:Xe/Kr solids.

Species	Band center (nm)	FWHM (eV)	τ_{rad} (ns)
XeF ($D\rightarrow X$)	303	0.1	10
XeF ($D\rightarrow A$)	364	0.23	10
XeF ($B\rightarrow X$)	428	0.07	a
XeF ($C\rightarrow A$)	575	0.4	80
KrXeF	465	0.24	80
Kr_2F	453	0.39	140
ArKrF[b]	343	0.48	60

[a] Excitation laser limited.
[b] For comparison (Ref. 7).

B. Emission spectra

Spectroscopic constants of the different emissions observed in F:Xe/Kr solids are collected in Table I. Emission spectra obtained by excitation at wavelengths between 308 and 380 nm are displayed in Fig. 4. The spectra are taken after extensive irradiation of the solid at 308 nm, and after several annealing cycles. Note that at these excitation wavelengths the KrF charge transfer resonances cannot be reached. The band assignment of the sharp emission at 428 nm to XeF ($B\rightarrow X$), and the broadband at 575 nm to XeF($C\rightarrow A$) is rather straightforward. In the gas phase these emissions appear at 351 and 450 nm,[21] while in solid argon they appear at 411 and 536 nm, respectively.[1,14,15] The large dielectric shift of these transitions is to be expected due to the ionic-to-covalent nature of the transitions, and follows the well established pattern of other solid state rare gas halides. There are in principle two possible assignments for the broad emission centered at 465 nm, these are: XeF($C\rightarrow X$) enhanced by interactions with neighboring Kr atoms, or emission from the mixed triatomic $(KrXe)^+F^-$ exciplex. The latter assignment is favored, as will be discussed.

It should be clear from Fig. 4 that the relative intensities of the different emissions are a strong function of excitation wavelength. The main absorption in this range of wavelengths is due to XeF($B\leftarrow X$). When excited at 308 nm, the $(KrXe)^+F^-$ emission dominates and the XeF($B\rightarrow X$) band appears as a small shoulder. When excited near the absorption threshold of 380 nm, the XeF($B\rightarrow X$) emission dominates the spectrum. The ratio between KrXeF and XeF ($C\rightarrow A$) remains independent of excitation wavelength.

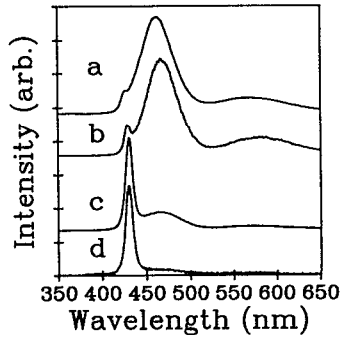

FIG. 4. Emission spectra from a F_2:Xe:Kr = 1:1:3000 solid taken with different excitation wavelengths: (a) 308 nm; (b) 351 nm; (c) 367 nm; (d) 380 nm. Prior to recording the spectra, the sample was subjected to extensive irradiation at 308 nm, and several annealing cycles. The spectral features are: 428 nm: XeF($B\rightarrow X$); 465 nm: $(KrXe)^+F^-$ and 575 nm: XeF($C\rightarrow A$). Note that Kr^+F resonances are not accessed.

However, the relative intensities of these emissions depend on temperature of the solid. Examples are shown in Fig. 5 for excitation at 250 nm, which corresponds mainly to XeF($D \leftarrow X$) absorption. It can be seen, that at elevated temperatures both $(KrXe)^+F^-$ and $C \rightarrow A$ intensities increase relative to the $B \rightarrow X$ transition. The temperature dependence of the relative populations of the XeF(C) and $(KrXe)^+F^-$ is also evident in the spectra.

Emission spectra obtained for excitation wavelengths between 232 and 275 nm are shown in Fig. 6. Here, the XeF($D \rightarrow X$) and ($D \rightarrow A$) emissions can be seen at 303 and 364 nm, respectively. Near the XeF($D \leftarrow X$) absorption threshold, at 275 nm, emission is observed almost exclusively from XeF(D), and the other weak emissions are at least in part due to reabsorption of the $D \rightarrow X$ and $D \rightarrow A$ emissions. Despite the fact that 275 nm excitation matches with the absorption maximum of the strong KrF($B \leftarrow X$) transition,[7] there is almost no contribution from $Kr_2^+F^-$ emission in the spectrum—all F atoms are scavenged by Xe trap sites under these conditions. Excitation high in the D manifold, leads to efficient internal conversion to populate the B/C and the KrXeF charge transfer states [see traces (a),(b), and (c) of Fig. 6].

A rather important observation made was that under intense pumping conditions over the XeF($B \leftarrow X$) resonance, emission from XeF(D) is observed. This is illustrated in Fig. 7, in which a strong emission at 303 nm is observed when the solid is pumped at 360 nm (pump fluence ~ 100 MW cm^{-2}). Comparison of the relative emission intensities, XeF($D \rightarrow X$), XeF($B \rightarrow X$), and $(KrXe)^+F^-$ in Fig. 7, indicates that the two-photon pumping scheme has a large cross section: the integrated intensity of the two-photon induced emission is comparable with the emissions due to the linear absorption. Although we have been able to demonstrate large gain, and amplified spontaneous emission on the XeF($D \rightarrow X$) transition when pumped at 260 nm,[3] efforts at observing laser action on the lower charge transfer states B, C, or KrXeF, by pumping at 351 nm were unsuccessful. A reabsorption cross section larger than the stimulated emission cross section, would explain the lack of gain on these transitions.

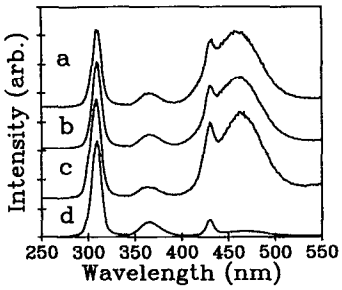

FIG. 6. Emission spectra from a F_2:Xe:Kr = 1:1:3000 solid at 15 K with different excitation wavelengths: (a) 232 nm; (b) 240 nm; (c) 250 nm; (d) 275 nm. Prior to obtaining the spectra, the crystal was subjected to annealing at $\sim$24 K. The emissions shown are: 303 nm:XeF($D \rightarrow X$); 364 nm:XeF($D \rightarrow A$); 428 nm:XeF($B \rightarrow X$), and 465 nm: $(KrXe)^+F^-$. The XeF($C \rightarrow A$) is not displayed.

C. Excitation spectra

The lamp excitation spectra of XeF($B \rightarrow X$), XeF($C \rightarrow A$), and KrXeF emissions are collected in Fig. 7. The bandpass of the excitation source is $\sim$2 nm. Excitation spectra recorded at higher resolution did not yield further structure in the spectra. The excitation spectra of XeF($C \rightarrow A$) and $(KrXe)^+F^-$ are almost identical: threshold near 380 nm and maximum at 343 nm. It should be noted, that in the case of $(KrXe)^+F^-$ emission, direct optical access of the emitting state is expected to be Franck–Condon forbidden since the difference in the Kr–Xe equilibrium distance between the shallow van der Waals ground state and the excited ionic states is $\sim$1 Å.[22] Thus for the most part, $(KrXe)^+F^-$ is expected to be formed via the diatomic states which can be directly accessed. No traces of vibrational structure is observed in these spectra. On the high energy side of the spectra, XeF($C \rightarrow A$) emission has a slightly broader excitation line shape. The inset in Fig. 8 shows a second weak excitation maximum of the $(KrXe)^+F^-$ emission. An identical peak is observed when XeF($C \rightarrow A$) is monitored.

The excitation spectrum of the XeF($B \rightarrow X$) emission peaks at 346 nm, and is red shifted from the other spectra. This difference is also evident in the emission measurements,

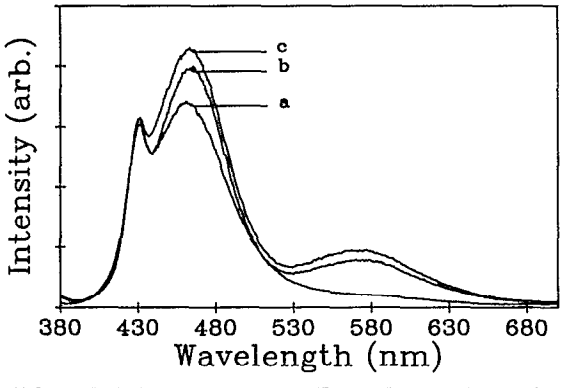

FIG. 5. Emission spectra from a F_2:Xe:Kr = 1:1:3000 solid at different temperatures: (a) 11 K; (b) 19 K; (c) 25 K. λ_{ex} = 250 nm. For band assignment, see Fig. 4. The XeF $D \rightarrow X$ and $D \rightarrow A$ emissions are not shown.

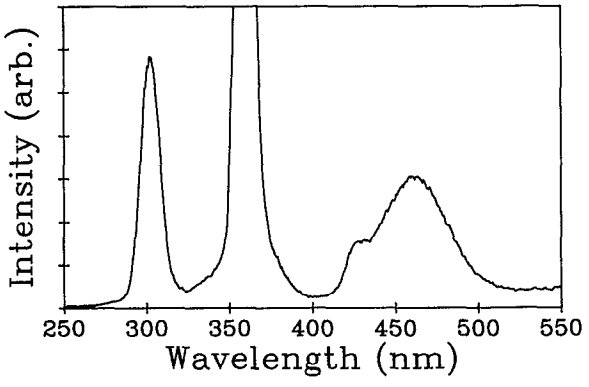

FIG. 7. Emission spectrum from a F_2:Xe:Kr = 1:1:3000 solid at 15 K under intense pumping conditions at 360 nm ($\sim$100 MW cm^{-2}). The 360 nm band is due to scattered laser light.

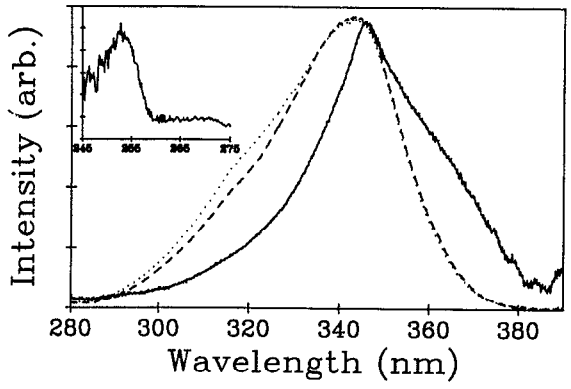

FIG. 8. Lamp excitation spectra from a F_2:Xe:Kr = 1:1:5000 free standing crystal. The emission monitored are: solid line: XeF($B \rightarrow X$); dashed line: $(KrXe)^+F^-$; dotted line: XeF($C \rightarrow A$). Monochromator slits correspond to 2 nm bandpass. Prior to recording the spectra, the crystal was subjected to overnight irradiation with broad band output of a Xe arc lamp. Inset shows a second excitation maximum (intensity ~15% of the main peak) in the XeF($C \rightarrow A$) and $(KrXe)^+F^-$ emission.

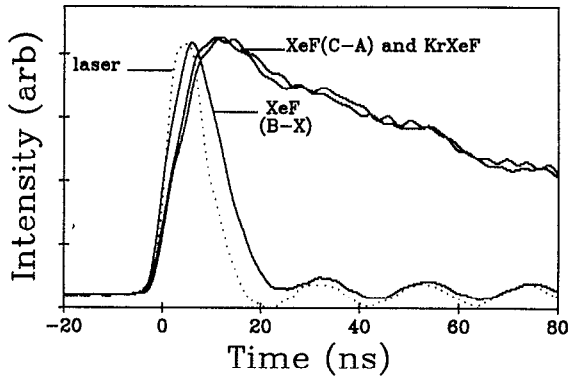

FIG. 10. Time profiles of XeF($B \rightarrow X$), XeF($C \rightarrow A$), and $(KrXe)^+F^-$ emission with 360 nm excitation. The original sample composition is F_2:Xe:Kr = 1:1:5000. The periodic oscillations in the signals are due to experimental artifact.

where excitation near the threshold region of XeF($B \leftarrow X$) yields almost pure $B \rightarrow X$ emission (see Fig. 4). This excitation spectrum possesses evidence of vibrational structure near threshold. Only two vibrational spacings 286 and 360 cm^{-1} are extracted. The $B \leftarrow X$ absorption threshold is estimated to be near 390 nm.

The excitation spectrum of the XeF($D \rightarrow X$) emission is presented in Fig. 9. This broad excitation profile does not yield any vibrational information. The strongly perturbed spectrum peaks at 260 nm and shows a valley at 252 nm. The sudden decrease in excitation efficiency of the D state near 255 nm, is directly correlated with the excitation resonance of the XeF($C \rightarrow A$) and $(KrXe)^+F^-$ emissions shown in the inset to Fig. 8. This information is also contained in the wavelength dependent emission spectra shown in Fig. 6. A crossing between the D state and the mixed triatomic charge transfer states nicely explains these observations.

D. Excited state kinetics

In Fig. 10 the time profiles of XeF($B \rightarrow X$), XeF($C \rightarrow A$), and $(KrXe)^+F^-$ emissions when excited at 360 nm, are shown. For timing purposes, the laser profile is also included. The XeF($B \rightarrow X$) emission is strongly convoluted with the pump pulse profile, as such the lifetime of the B state cannot be extracted with any confidence. The XeF($C \rightarrow A$) and $(KrXe)^+F^-$ emissions rise promptly and both relax with a fluorescence lifetime of 80 ns. This lifetime is independent of temperature (12–26 K), composition (1:1:3000–1:1:10,000) and excitation details; as such, it can confidently be assumed to be controlled by radiation. The small difference in rise of XeF(B) vs XeF(C) and KrXeF can be explained by convolution of decay times in the rise.

Figure 11 shows the time profiles of XeF($D \rightarrow X$) and XeF($C \rightarrow A$) emissions when the D state is excited directly. Although the time evolution of the D state emission is strongly convoluted with the laser pulse, a decay rate of 10 ns can be extracted by kinetic deconvolution as will be discussed. As in the case of excitation to the B state, excitation into the D manifold results in identical time profiles for XeF($C \rightarrow A$) and $(KrXe)^+F^-$ emissions. However, in contrast to the 360 nm excitation, excitation to the D manifold leads to a finite risetime in these emissions; moreover, this delay depends on the excitation wavelength as illustrated in Fig. 11. While the risetime in the case of 250 nm excitation can be attributed entirely to deconvolution of the laser pulse, the delay in the rise for 260 nm excitation implicates an intermediate state which feeds into the lower manifold on a time scale of 10 ns. These excitation wavelengths correspond to the dip and peak observed in the excitation spectrum of the D state (see Fig. 9).

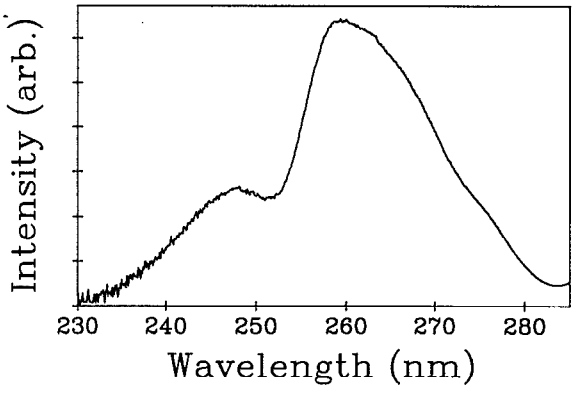

FIG. 9. Lamp excitation spectrum of the XeF($D \rightarrow X$) emission. For experimental details, see Fig. 8.

IV. DISCUSSION

A. Long-range migration

The major finding of the photogeneration studies in these ternary F_2:Xe:Kr solids is that the fraction of F atoms that reach Xe sites is a strong function of photodissociation wavelength. Since Xe centers act as scavengers for thermally mobile F atoms in Kr, probing the XeF number densities during photodissociation and subsequent to warmup of the

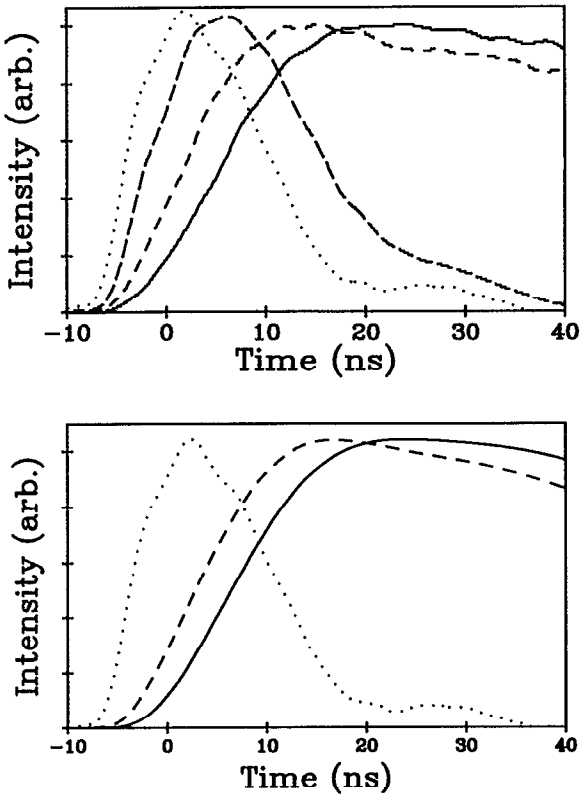

FIG. 11. Top panel: Time profile of the XeF($C \rightarrow A$) emission. Short dashed line: 250 nm excitation; solid line: 260 nm excitation. Long dashed line represents the time profile of the XeF($D \rightarrow X$) emission. Included is also the temporal profile of the exciting laser pulse (dotted line). Lower panel: simulated risetime of the XeF($C \rightarrow A$) emissions according to Eq. (2) (solid line) and Eq. (3) (dashed line). For parameters used in the simulations, see text. Dotted line shows the time profile of the laser.

solid, could, in principle, yield the fraction of F atoms that reach Xe sites during photodissociation. However, the present data are not sufficient to accurately determine this fraction since the F atom loss channels due to F + F recombination, and due to formation of XeF_2 are unaccounted. Despite this shortcoming, important conclusions can be reached from the experimental observations that: at dissociation wavelengths of 351 nm and longer, of the F atoms that survive the heating cycle only $\sim 0.2\%$ were initially produced next to Xe; while in the same solids, when the dissociation is carried out at 308 nm and shorter wavelengths, this fraction corresponds to 10%–20%. The fraction observed in the long wavelength limit can be well rationalized on the basis of the statistical probability of isolating an F_2 molecule next to Xe. Thus for substitutionally trapped guests in an fcc lattice, the number of dimeric guests can be calculated as: $N_D = 12Np^2(1-p)$,[18] in which N is the total number of sites and p is the guest mole fraction.[23] For the typical doping densities used in the present studies of F_2:Xe:Kr = 1:1:3000, the fraction of F_2 molecules that will isolate next to Xe can be calculated as $N_D/(Np) = 4 \times 10^{-3}$ (0.4%). The close agreement of this value with that of 0.2% observed experimentally, leads us to two important conclusions: (a) The initial molecular distribution in these free standing crystals is essentially statistical, (b) The F atoms produced by dissociation at 351 nm and longer wavelengths (photodissociation excess energies < 1.9 eV), remain near the original trapping site of the parent. The 2 orders of magnitude increase in the fraction of F atoms which reach Xe sites when the dissociation is carried out at shorter wavelengths, can only be explained as due to long-range migration of the F atoms upon the initial photodissociation impulse. Since it was argued above that initial molecular distributions are statistical, a migration range comparable to the average separation between F_2 and Xe of ~ 15 lattice sites is implied for dissociation at wavelengths between 308 and 260 nm (photodissociation excess energy > 2.4 eV). While the fraction of photodissociation events that lead to long-range migration is not ascertained, the effects of impulsive cage exit, and subsequent impulsive migration of F atoms is clearly established by these studies. Finally, we note that the good agreement between the statistical probability of F_2:Xe isolation with the fraction of XeF observed after long wavelength dissociation, would further imply that at the lower excess energies the F atom migration is extremely limited.

Impulsive cage exit and subsequent long-range migration of F atoms was recently discovered in molecular dynamics simulations of F_2 photodissociation in crystal argon.[6] The strongly guided migration of F atoms in the lattice is unique to this system, and has not been observed in related simulations of H and Cl trajectories in solid Xe.[24,25] Out of 50 trajectories simulated at each energy, long-range migration of F atoms was observed at the two highest energies used in the simulation: one trajectory at an excess energy of 2.0 eV, four trajectories at 2.8 eV. Due to the limited size of the lattice used in the simulations, the range of migration could only be estimated as ~ 10 lattice sites. Despite the fact that the simulations were carried out for solid argon and the experiments discussed are in solid Kr, the agreement between the two is satisfactory with respect to both the threshold of this process, and the range of flight of the F atoms. As discussed above, it is more difficult to compare the probabilities of such trajectories except in a semiquantitative fashion. We suffice by indicating that at the theoretical threshold of 2 eV, $\sim 10\%$ of the trajectories undergo long-range migration. Experimentally it is observed that for excess energies of 2.4 eV, of the F atoms that survive the heat cycle between 10% and 20% reached Xe sites; which would imply order-of-magnitude agreement between experiment and theory.

B. Charge transfer states

1. Diatomic states

The spectroscopy of a variety of rare gas halide exciplexes in X/Rg/Rg′ ternary solids were reported in an early study by Ault and Andrews.[14] This was followed by a detailed study of photodynamics in XeF doped solid argon and neon by Goodman and Brus.[15] Also relevant to the present are the liquid phase studies of rare gas fluorides,[26] and the vast literature on gas phase studies of rare gas halide exciplexes.[27] In solid Ne, vibrationally resolved spectra with clear zero-phonon lines are observed in both excitation and emission over the XeF(D–X) transition—the emission max-

imum is assigned to the $v' = 0$–$v'' = 2$ transition, at 270 nm. The vibrational assignment also corresponds to the Franck–Condon maximum of this transition in the gas phase which occurs at 265 nm.[28] In solid Ar, the $D \rightarrow X$ emission is further shifted to 287 nm, shows no vibrational structure, and decays with a radiative lifetime similar to that in the gas phase of 11 ns.[15] The structureless, but relatively sharp emission at 303 nm in Kr, which decays with a radiative lifetime of 10 ns, can confidently be assigned to XeF($D \rightarrow X$). Although weak, the same transition is also observed in liquid Kr at 312 nm.[26] Due to the repulsive nature of the A potential, a broad $D \rightarrow A$ emission is expected to accompany the $D \rightarrow X$ transition. While this is clearly observed in both solid Ar and solid Kr, at 345 and 365 nm, respectively; it was surprisingly reported to be absent in solid Ne.[15] If we assume that the $D \rightarrow X$ transition in Kr also terminates on $v'' = 2$ of the X potential, then a spectral shift of 0.59 eV is observed between the gas and solid state. This shift is attributed to the ionic-to-covalent nature of the transition, in which the giant dipole of the excited state is solvated by polarization of the medium. That the main contribution to the shift is due to lowering of the upper state is consistent with the observation that the differential shifts between Kr and Ar for the $D \rightarrow X$ and $D \rightarrow A$ transitions are nearly identical—0.21 and 0.19 eV, respectively. However, it will be argued below that significant stabilization of the ground state is also expected, and necessary to interpret the data consistently.

While the XeF($B \leftarrow X$) and ($C \leftarrow X$) absorptions have been characterized in Ne, direct optical access of these states did not yield any radiative relaxation via the expected $B \rightarrow X$ and $C \rightarrow A$ channels.[14,15] The absence of emission from the B state could be rationalized as due to a change in the ordering of B and C states in Ne as compared to the gas phase, with the additional stipulation of strong coupling between $v = 0$ of B and the C state. However, this explanation makes the reported absence of $C \rightarrow A$ emission difficult to rationalize. In Ar, the $B \rightarrow X$ emission peaks at 411 nm, decays with a radiative lifetime of 6 ns, and shows partially resolved vibrational structure.[15] The vibronic transitions are broadened and overlap, making definite assignments difficult. In Kr this transition further shifts to 428 nm, and as in the case of $D \rightarrow X$ in Ar, shows no vibrational structure. The fluorescence decay over this transition is laser limited, however consistent with a lifetime of ~ 5 ns. The differential shift between Kr and Ar of 0.12 eV for this transition is significantly smaller than that observed for the D state. The spectral range in which this transition occurs is congested in liquid Kr by emissions from Kr_2F and possibly KrXeF, and the assignment of 475 nm to $B \rightarrow X$ by spectral deconvolution may not be very reliable.[26]

The broad $C \rightarrow A$ emission which decays with a radiative lifetime of 120 ns can be clearly observed at 536 nm in Ar. Prior confusion about this assignment was based on the observation of variation in the relative intensities of the $B \rightarrow X$ and $C \rightarrow A$ emissions.[15] This variation can be ascribed to differences in nonradiative relaxation cross sections of the B and C states when isolated near impurities other than Ar[1]—an experimental difficulty that cannot be avoided in these systems since the exciplexes are prepared *in situ*, by photodissociation of an F atom donor. With the aid of delayed gated detection, the long lived $C \rightarrow X$ emission has been isolated at 407 nm in Ar to further verify this assignment.[29] In Kr, the broad emission at 575 nm is assigned to $C \rightarrow A$, which is consistent with 550 nm assignment for this transition in liquid Kr.[26] The differential shift of 0.16 eV between Ar and Kr for this transition is in accord with that of the $D \rightarrow A$ transition. Finally, in F doped solid Xe, emission only from Xe_2F is observed, however, the excitation spectra could be simulated as the envelopes of the $B \leftarrow X$, $D \leftarrow X$ absorptions.[10]

While this completes the spectroscopic assignments of the diatomic XeF charge transfer transitions in rare gas solids, significant uncertainty remains as to the exact locations of the different potentials which are key to the understanding of both energy transfer and molecular dynamics. This task is made difficult by the absence of vibrational structure in the transitions observed in Kr. We therefore concentrate on analysis of the bound-to-repulsive transitions with two reliable assumptions kept in mind: (a) It is assumed that gas phase pair potentials are a fair representation for the section of the A potential of concern, since this corresponds to a repulsive surface ~ 0.5 eV above ground; (b) It is assumed that the $v = 0$ wave functions in the different ionic states are well represented by Gaussians with harmonic frequencies identical to those of the gas phase. For the simulations, the experimental potentials of Aquilanti *et al.*[19] for the A state are used. In the range of interest, the potential is well fit to an exponential with amplitude $A = 19\,798$ eV and steepness $\alpha = 4.15$ Å^{-1}. It is then possible to simulate the bound–free spectra by reflection of a Gaussian from an exponentially repulsive wall:[30]

$$I(\bar{v}) = \frac{B^{2}}{\alpha(E_0 - \bar{v})} \times \exp\left\{ -\beta \left[\frac{1}{\alpha} \ln\left(\frac{\alpha}{E_0 - \bar{v}} \right) - r_0 \right]^2 \right\} d\bar{v}, \qquad (1)$$

in which $\bar{v}$ is the transition energy in wave numbers; $E_0 = T_0 + \omega_e/2$ is the zero point energy of the excited state; A and α are the amplitude and steepness of the exponentially repulsive XeF(A) state; B and β are, respectively, the normalization constant and the width of the upper state Gaussian wave function; and r_0 is the equilibrium bond length of the excited state. For the C state, $\omega_e = 346$ cm^{-1} and $r_0 = 2.45$ Å are adapted from gas phase data;[21] whereas for the D state, $\omega_e = 316$ cm^{-1} is taken from matrix isolation studies[14] and a trial $r_0 = 2.5$ Å is used as a starting point for the $D \rightarrow A$ line shape. The electronic energy E_0 of the excited state is left as a free parameter to match the emission maximum, and the equilibrium distance of Xe^+F^- is varied to match the width.

In Fig. 12 the simulated $D \rightarrow A$ and $C \rightarrow A$ emission profiles are superposed with the experimental spectra. The baseline in the experimental $D \rightarrow A$ emission is due to partial overlap with the $D \rightarrow X$ and $B \rightarrow X$ emissions; the $C \rightarrow A$ line shape is overlapped by the tail of the strong $(KrXe)^+F^-$ emission. The best fit for the $D \rightarrow A$ emission is obtained with $E_0 = 3.8$ eV and $r_0 = 2.59$ Å, the emission terminating with 0.425 eV of repulsive energy on the A surface. The obtained

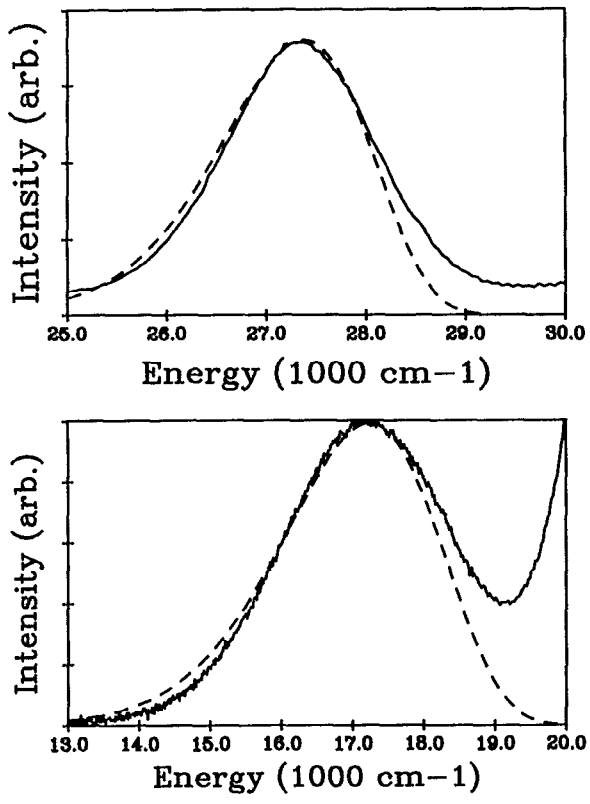

FIG. 12. Top panel: XeF($D \rightarrow A$) emission with 275 nm excitation. The original sample composition is F_2:Xe:Kr = 1:1:3000. The nonzero baseline is due to partial overlap by XeF($D \rightarrow X$) and XeF($B \rightarrow X$) emissions. Dashed line represents the line shape obtained from the classical reflection treatment. Lower panel: XeF($C \rightarrow A$) emission with 308 nm excitation. On the high energy side the emission is overlapped with that of $(KrXe)^+ F^-$. Dashed line shows the simulated emission profile.

bond length is in acceptable agreement with the *ab initio* prediction of 2.62Å.[31] However, the electronic origin of the XeF(D) is not consistent with the experimental $D \rightarrow X$ emission spectrum. Based on the assumption of a Morse potential, Goodman and Brus report 0.15 eV binding of XeF(X) isolated in solid neon, a nearly 30% increase in binding energy as compared to the gas phase.[28] Adding this, and the spin–orbit splitting in F of 0.05 eV to the determined E_0 value, the $D \rightarrow X$ (0,0) transition would be placed at 308 nm, while the experimental value is 303 nm. In order to make the energetics consistent, an additional ~0.1 eV contribution is needed for the binding of the ground state. This is quite reasonable if we note that the ground state potential should be given as a sum over all nearest neighbors and that the binding energy of KrF(X) in the gas phase is 0.016 eV.[19,20] The ground state potential in this case should be strongly perturbed, and given the narrow, structureless $D \rightarrow X$ emission, it is safe to assume that at the excited state minimum of ~2.6 Å the ground state surface is nearly flat. Little information is obtained from the excitation spectra of the D state as to its energetics. The excitation threshold of ~4.35 eV, would imply that the D state minimum is significantly shifted to longer bond length than the X state minimum which is near 2.3 Å in the gas phase.

The best simulated line shape for the $C \rightarrow A$ emission is obtained with $E_0 = 2.75$ eV and $r_0 = 2.48$ Å. The equilibrium distance compares favorably with the gas phase estimate of 2.45 Å.[21] Thus the radiative dissociation of XeF(C) would lead to creation of neutral atoms with ~0.7 eV of repulsive energy. This energy was experimentally verified to be sufficient for F atom cage exit in F:Xe/Kr and F:Xe:Kr/Ar solids.[7,8] Since the $B \rightarrow X$ emission does not possess any vibrational structure, and the (0–0) absorption of the $B \leftarrow X$ is not observed, it is difficult to estimate the exact location of the B state. If, as in the gas phase and as in solid Ar, the peak of the $B \rightarrow X$ emission at 2.9 eV is taken to terminate at $v'' = 3$ of the X potential, the electronic origin of the B state would be at 2.82 eV. This treatment would place the C state 580 cm^{-1} below the B as compared to 775 cm^{-1} observed in the gas phase.[21] However, if we assume that the ground state is further lowered due to F–Kr interactions by an additional 0.1 eV as concluded above, then the B state would be located at 2.72 eV, i.e., below the C state by one vibration. The observation of $C \rightarrow X$ emission to the blue of the $B \rightarrow X$ emission in solid Ar, would indicate that C is above B in Ar as well. The two states may very well be in accidental resonance in solid Ne, which could perhaps explain the absence of B or C emissions there. In summary, the limited information provided by the emission spectra, indicate that the ionic potentials of diatomic XeF in solid Ar and solid Kr maintain a close similarity with the gas phase, however, given the large spectral shifts of ~0.5 eV, differential solvation and even a change in the ordering of B and C states is suspected. As far as the ground state of XeF is concerned, given the absence of any vibrational structure or even a Franck–Condon contour on emissions terminating in the X state, we conclude that the potential is strongly perturbed by many-body Kr–F interactions.

2. Triatomic states

The broad, long-lived emissions at 453 and 465 nm in Kr do not have a direct relation to diatomic XeF states. The first of these develops when the sample is irradiated at low temperatures, and disappears upon warmup. Its line shape, and lifetime are nearly identical to the only emission observed in F/Kr solids, and can therefore be confidently assigned to Kr_2F. This bound-to-free transition has been previously analyzed in some detail by the reflection approximation, with the conclusion that most of the spectral width, therefore repulsion on the lower surface, is due to the Kr–Kr coordinate.[7]

The broad emission at 465 nm grows with annealing at the expense of loss in the Kr_2F emission. The emission is therefore due to F atoms deeply bound in the ground state, evidently due to trapping as nearest neighbors to Xe. Moreover, the upper state responsible for this emission is strongly coupled with XeF(C), since it shows the same fluorescence lifetime and tracks the XeF($C \rightarrow A$) intensity at all excitation wavelengths. Since the XeF(C) state maintains its integrity, the present emission is clearly due to a distinct charge transfer complex, as opposed to XeF(C) perturbed by Kr. Given the spectral width of this emission, assignment to $C \rightarrow X$ can-

not be justified. The mixed triatomic $(KrXe)^+F^-$ is the alternate assignment. Since the XeF(C) and KrXeF charge transfer states are in thermal equilibrium at these cryogenic temperatures, the two states must be isoenergetic, presumably separated by a small barrier. Although several mixed triatomic rare gas halide exciplexes have been characterized in the gas phase,[32] KrXeF has not been identified. A possible reason for this failure may be the fact that the more stable Kr_2F emission occurs in the same spectral range, which would be present in gas mixes designed to produce the mixed triatomic. The same difficulty exists in liquid Kr.[26]

The observation of equilibrium between XeF and KrXeF raises important questions about structure and stability of charge transfer configurations in these solids. In binary X/Rg solids, no emission from diatomic charge transfer states can be observed. The optically accessed states rapidly relax to the lowest energy charge transfer configuration which is usually the triatomic Rg_2X exciplex. This has been amply demonstrated for all halogen atoms trapped in Xe,[30] for F[8] and Cl[33] trapped in Ar, and for all halogen atoms trapped in Kr.[13] Since the data on the latter is scattered in the literature, we provide in Table II the emission peaks, widths, and lifetimes of all solid state Kr_2X species observed in our laboratory. The ternary X/Rg/Rg′ solids provide a more subtle balance of energetics and dynamics. As discussed above, in such solids as F/Xe/Ar and F/Xe/Ne, the only observed exciplexes are those of the diatomic XeF. Similarly, only the diatomic ArCl and KrCl exciplexes are observed in Cl/Ar/Ne and Cl/Kr/Ne solids.[17] In contrast with these solids, only the mixed triatomic ArKrF exciplex is observed in F/Kr/Ar.[7] In Cl/Xe/Ar, Cl/Xe/Ne, as in the present, emission from both mixed triatomic NeXeCl, ArXeCl, and diatomic XeCl states are reported.[17] Which diatomic exciplexes can be isolated in a given rare gas host? Or equivalently, what prevents the formation of RgRg′X mixed triatomic exciplexes in ternary X/Rg/Rg′ solids? The binding in Rg^+X^- is predominantly Coulombic, as such it would be expected that as long as the $(RgRg')^+$ ion is bound, the mixed triatomic exciplex would be lower in energy. This consideration is well justified for the deeply bound diatomic rare gas ions. A good correlation can be made between the binding energies of $(RgRg')^+$ and the spectral shift between RgX and RgRg′X exciplexic emissions observed in the gas phase, as seen in Table III. The stabilization energies of the triatomic exciplexes relative to their diatomic counterparts is even better correlated with binding energies of the rare gases than the spectral shifts would indicate, since a significant contribution to the observed spectral shift is due to increased repulsion on the Rg–Rg′ coordinate of the triatomic ground states. According to the relative emission intensities, and their temperature dependence, the KrXeF and XeF(C) states are within ~ 20 cm^{-1} in energy, yet the binding energy of $KrXe^+$ is 0.385 eV. $ArXe^+$ is bound by 0.176 eV, yet XeF in Ar remains as the stable exciplex. Clearly, the binding energy of $(RgRg')^+$ is not sufficient to determine the stability of the mixed triatomic exciplex relative to the diatomic. The nature of the halogen ion can significantly alter the stability of a particular charge configuration. For example, while XeF is stable in Ar, ArXeCl and XeCl coexist in Ar,[16,17] and in Br/Xe/Ar the only observed emission should be assigned to ArXeBr.[14] Therefore, in the case of $(ArXe)^+X^-$, the stability relative to Xe^+X^- increases in the series F, Cl, Br. It is possible to rationalize this correlation by the extent of charge localization in the ionic counterparts. The localization of charge in F^- would be expected to favor hole localization on a single atom thus favoring the formation of diatomic exciplexes. Larger halides may accommodate more diffuse hole wave functions that are presented in diatomic rare gas ions. To complete such arguments in dense media, host polarizabilities and lattice relaxation energies need to be taken into account. The subtle balance in energetics provided by these considerations can be discerned by comparing the stabilities of these charge transfer states in different phases. As an example, in the case of Cl/Xe/Kr, in the solid state the main emission is due to Xe^+Cl^-,[30] while in the liquid phase only $(KrXe)^+Cl^-$ is observed.[16] Presumably, the lattice relaxation energy required to stabilize the triatomic is too prohibitive in the solid state. A more rigorous treatment of energe-

TABLE III. $(RgRg')^+X^-$ and Rg'^+X^- emissions in gas phase.

$(RgRg')^+X^-$	Center (nm)	Rg'^+X^- ($B\rightarrow X$)	ΔE(eV)[a]	D_0(eV)[b]
Ar_2F	292[c]	193	2.17	1.269
Kr_2F	400[d]	248	1.9	1.150
Kr_2Cl	325[c]	221[e]	1.8	1.150
Xe_2F	610[f]	351	1.5	1.03
Xe_2Cl	490[f]	308	1.5	1.03
ArKrF	305[d]	248	0.9	0.528
ArKrCl	270[d]	221[e]	1.0	0.528
KrXeCl	370[d]	308	0.68	0.385
KrXeF	428[g]	465[g]	0.2	0.385
ArXeF		not observed		0.176

[a] ΔE is the difference between the triatomic and the Rg'^+X^- ($B\rightarrow X$) emission centers.
[b] D_0 is the binding energy of the corresponding $(RgRg')^+$ ion (Ref. 35).
[c] Reference 32.
[d] Reference 30.
[e] Reference 33.
[f] Reference 34.
[g] Solid Kr numbers, not observed in the gas phase.

TABLE II. Emission bands of solid state triatomic krypton halides (Kr_2X).[a]

	Emission peak (nm)	FWHM (eV)	Radiative lifetimes (ns)
Kr_2I	280	0.38	210
Kr_2Br	320	0.38	220
Kr_2Cl[b]	355	0.38	217
Kr_2F[c]	463	0.39	140

[a] For emission spectra see Ref. 13.
[b] Reference 16.
[c] Reference 17.

tics in these systems is clearly warranted for both practical and fundamental considerations, at present we suffice by noting these general correlations. Instead, we concentrate on the details of dynamics between the different ionic states in the particular example of F/Xe/Kr.

An estimate of the location of the $(KrXe)^+F^-$ potential minimum is useful for the rationalization of the observed dynamics in this system. Previously, the emission line shapes of the different Xe_2X (X = F, Cl, Br, I) species have been analyzed by a two dimensional reflection approximation.[30] The FWHM of these emissions was observed to be quite independent of the halogen, dominated mainly by the potential gradient along the Xe–Xe coordinate on the ground surface. Similar considerations apply for the triatomic krypton halides which show similar line shapes (see Table I), and spectral analyses of Kr_2F and Ar_2F have previously been presented.[7,8] In the present, the energy of the ionic upper state of KrXeF is fixed by the observed interconversion equilibrium at 2.75 eV. Given the 0.5 eV blueshift of the triatomic emission relative to $XeF(C\rightarrow A)$, which terminates at $\sim$0.7 eV above the separated atom limit, it is possible to infer that the triatomic emission terminates at $\sim$0.2 eV above ground. Attributing this repulsive energy strictly to the Kr–Xe coordinate, and using Kr–Xe pair potentials, it can be concluded that the $KrXe^+$ minimum occurs near 3.3 Å (the van der Waals distance of KrXe is 4.2 Å).[36] In comparison with the minima of the more strongly bound homonuclear ions—3.17 Å[37] for Xe_2^+ and 2.79 Å[38] for Kr_2^+—it is clear that $KrXe^+$ is less tightly bound, nevertheless, the formation of the triatomic exciplex involves a significant bond compression along the Kr–Xe coordinate. The similarity of emission line shapes of KrXeF and Xe_2F can be simply rationalized by the similarity of ground state Kr–Xe and Xe–Xe potentials in the 3.0–3.4 Å range.[39] Thus the formation of the triatomic charge transfer configuration, which is directly correlated with $XeF(C)$, involves a significant lattice relaxation: large compression of the KrXe separation along with elongation in the F–Xe coordinate. This interconversion must be accompanied by an adiabatic barrier, i.e., the excited ionic surface must contain two well defined minima, in order to sustain the two well defined emissions assigned to the triatomic and diatomic configurations. The two configurations relax with the same fluorescence lifetime of 80 ns, and therefore interconvert on a time scale shorter than $\sim 10^{-9}$ s. The observed lifetime is in line with the radiative lifetime of ArKrF of 60 ns, and shorter than what would be expected for $XeF(C)$, which has a radiative lifetime of 120 ns in Ar. It is therefore possible to rationalize that the decay of these coupled states is controlled by the purely radiative lifetime of the triatomic. It is remarkable to observe that these states, in their vibrational ground states, are completely decoupled from $XeF(B)$. However, it is also clear from the excitation spectra that the vibrationally excited states of $XeF(B)$ are strongly coupled to C and KrXeF.

C. Excited state kinetics

The lack of vibrational structure in the excitation spectra could have its origins in both a strong coupling of the ionic excited state to lattice phonons, and an efficient energy transfer from the optically accessed states to the neighboring charge transfer manifold. Spectral broadening due to coupling to phonons alone would not be expected to have a strong dependence on vibrational states, and a Franck–Condon analysis based on the gas phase potential parameters is to be expected to reproduce at least the envelope of the excitation spectra (see, e.g., the cases of XeF in solid Xe,[10] and KrF in solid Ar.[7]) The spectra in the present are strongly perturbed and could not be expected to be reproduced by considering diatomic coordinates alone. The complicated coupling between the nested diatomic and triatomic charge transfer potentials is most pronounced in the excitation spectrum of the $XeF(D\rightarrow X)$ emission where a minimum is observed at $\sim$252 nm, coincident with the onset of excitation into the $XeF(C)$ and KrXeF states. A crossing between $XeF(D)$ and the mixed triatomic charge transfer potentials is an obvious source of this perturbation, a proposition which is further supported by the wavelength dependence of fluorescence rise times in the lower charge transfer manifold.

It should be clear from Fig. 11, that there is a finite delay in the population rise in $XeF(C)$ when the D state is accessed at 260 nm, as compared to excitation at 250 nm, which corresponds to the dip in the excitation spectrum of the D state. The delayed rise in population can be simulated by assuming fast vibrational relaxation in the D state, and a slow crossover to the lower charge transfer manifold. A minimal kinetic model that can reproduce both the delayed rise in the C state and the time profile of the D state could be presented as:

$$XeF(X) + h\nu(260\ \text{nm}) \rightarrow XeF(D, v = v^*), \tag{2a}$$

$$XeF(D, v = v^*) \rightarrow XeF(D, v = 0) \quad \text{fast}, \tag{2b}$$

$$XeF(D, v = 0) \rightarrow XeF(X) + h\nu \quad k_1, \tag{2c}$$

$$XeF(D, v = 0) \rightarrow XeF(C) \quad k_2, \tag{2d}$$

$$XeF(C) \rightarrow XeF(A) + h\nu \quad k_3. \tag{2e}$$

The fast relaxation in Eq. (2a) is accounted by assuming that $v = 0$ is directly pumped by the laser pulse, and therefore the laser pulse profile is directly integrated to simulate the population rise in D. For the radiative relaxation rates, $k_3 = 0.012\ \text{ns}^{-1}$ is directly obtained from the fall times. For a choice of $k_1 = k_2 = 0.1\ \text{ns}^{-1}$, both the $XeF(D, v = 0)$ time profile, and $XeF(C)$ rise are reproduced (see Fig. 11). It is not possible to simulate the C state time profile for 250 nm excitation with the same model. Direct pumping of the C state, with rapid vibrational relaxation in the C manifold are required to reproduce the fluorescence rise in this case. The kinetic model used in this simulation can be summarized as:

$$XeF(X) + h\nu(250\ \text{nm}) \rightarrow XeF(C, v = v^*), \tag{3a}$$

$$XeF(X) + h\nu(250\ \text{nm}) \rightarrow XeF(D, v = v^*), \tag{3b}$$

$$XeF(C, v = v^*) \rightarrow XeF(C, v = 0) \quad k. \tag{3c}$$

A vibrational relaxation rate constant, $k = 100\ \text{ns}^{-1}$ is necessary to reproduce the population rise in the C state, as shown in Fig. 11. It should be noted that in the above models it is implicitly assumed that $XeF(C)$ and KrXeF are in fast equilibrium; the present experiments do not distinguish between these two states. These simulations are used to re-

enforce the interpretation that the dip in the D state excitation spectrum corresponds to a crossing with a charge transfer potential closely connected with the states of the lower manifold. The most likely candidate for such a crossing is the triatomic exciplex.

As shown in Fig. 9, when the solid is excited at 360 nm, the strongest emission is observed to emanate from the D state, at 303 nm. The D state emission in this case is clearly due to a two-photon absorption. In several prior studies on condensed phase triatomic rare gas halides, failure to observe laser action was attributed to reabsorption from the $4^2\Gamma$ state. The same process has been characterized in gas phase Kr_2F and Xe_2Cl in which the main reabsorptions are assigned to $9^2\Gamma \leftarrow 4^2\Gamma$.[40] It has been shown in the gas phase, that reabsorption leads to dissociation of the triatomic and emission from diatomic (B,C) states. A continuum of charge transfer states with possible delocalization of the hole can serve as the upper state of such an absorption in the solid state. However, to date, these states have defied analysis. The present system is the first example in which the reabsorption results in a clear signal that can be monitored to elucidate the nature and spectroscopy of the ionic states near the charge separation continuum. Such studies are planned. Here, we note that the absence of gain on the lower manifold of charge transfer states would imply that the reabsorption cross section is much larger than the stimulated emission cross section of KrXeF which can be estimated to be $\sim 2\times 10^{-17}$ cm^2. It is important to note that although the reabsorption is attributed to KrXeF, it also suppresses emission from the B and C states. Equilibrium between C and KrXeF explains the latter. However, since XeF(B, $v=0$) is not coupled to the triatomic states, suppression of the B state emission would only be possible if vibrational relaxation in this state occurs through a cascade with a bottleneck in the neighboring electronic manifold. Note that this would require a reabsorption rate that could compete with vibrational relaxation, therefore much larger than the limit set by the stimulated emission cross section of KrXeF. Further studies of these processes are required.

V. CONCLUSIONS

Impulsive, long-range migration of F atoms was discovered as a unique trait of F_2 photodissociation in rare gas solids by molecular dynamics simulations.[6] That prediction was verified in the present study. Migration of F atoms is observed to take place over a distance of ~ 15 lattice sites in solid Kr when the dissociation is carried out at excess energies above 2.4 eV. At photodissociation excess energies below 1.9 eV, the F atoms remain within the vicinity of the initial molecular site. These observations are in good agreement with theory. The technique introduced for these measurements, namely double doping of the solid with the molecular impurity and a scavenger of the atomic fragments could be applied with variations to a host of solid state dynamical measurements. A most fascinating prospect for this methodology is its potential in real time applications. Using short laser pulses, it should be possible to measure the arrival time of fragments at the scavenger sites—a solid state time of flight measurement. Finally, it is important to note that photomobility of F atoms in both Ar and Kr solids had previously been noted in experimental studies, although the emphasis in those studies had been on photomobility induced by radiative dissociation of exciplexes.[1,7,8] Thus several different mechanisms lead to extensive mobility of F atoms in cryogenic RGS, and therefore F atoms are well suited for bimolecular chemistry in these media.

A large number of solid state rare gas halide exciplexes have been identified in the past few years. These seemingly simple species, charge transfer complexes of atomic solids doped with atomic impurities, show a rich variety of behavior worthy of theoretical scrutiny. Some progress in this direction has been made, in particular by Last and George.[41] Ternary X/Rg/Rg′ solids should present a more rigorous test of theories due to the subtle balance of energetics between diatomic and triatomic charge transfer configurations. From correlations between the stability of different ionic states, and the observed mixed triatomic exciplexes in condensed phases, some simple conclusions can be made. Thus although all $(RgRg')^+$ ions are bound, this does not imply that the mixed triatomic exciplexes are more stable than their diatomic counterparts in solids. The exclusive isolation of XeF in solid Ar is a counterexample. In a given series, the heavier the halogen ion, the more stable the mixed triatomic configuration—$(ArXe)^+Cl^-$ is observed in equilibrium with Xe^+Cl^-,[17] and it seems that $(ArXe)^+Br^-$ is the exclusive emitter in Br/Xe/Ar solids.[14] In the present we find that the XeF(C) and KrXeF charge transfer configurations are in dynamic equilibrium, while XeF(B, $v=0$) which is separated from these states by only a few vibrations remains completely uncoupled. Some information about these multidimensional potentials is obtained from the analysis of spectral line shapes, and in particular, by the observation of a crossing between XeF(D) and KrXeF surfaces. However, due to the absence of vibrational structure in the excitation and emission spectra in F/Xe/Kr solids, significant uncertainty remains as to the exact locations and shapes of excited and ground state potentials. The energetics and dynamics of these charge transfer states are clearly relevant to developments of solid state exciplex lasers. Laser action was recently demonstrated on the XeF($D \rightarrow X$) transition in solid Kr when pumped at 260 nm.[3] The efficiency of this process can now be understood. When pumped at 260 nm, nonradiative transfer from the D state to the lower manifold proceeds on a time scale of 10 ns, the same as the radiative relaxation time scale of the D state. Thus $\sim 50\%$ of the population relaxes radiatively, in effect, XeF(D) can be assumed to be isolated from the lower manifold of charge transfer states. In contrast with the D state, gain has not been observed from the lower manifold of charge transfer states. In fact, under strong pumping conditions over the XeF($B \leftarrow X$) transition, emission is observed from the D state due to two-photon absorption. Thus clearly, a very strong excited–excited absorption competes favorably with stimulated emission cross sections in the lower manifold of charge transfer states. This mechanism had in the past been postulated to explain the lack of laser action on all previously attempted condensed phase triatomic exciplex lasers, yet no direct proof had been obtained. Note that although the XeF(B,

$v = 0$) is isolated from XeF(C) and the triatomic states, the reabsorption suppresses the B state population as well. This would indicate that vibrationally excited states in B are strongly coupled to the neighboring states, which is also verified by the excitation spectra monitoring the different emissions in the system. The very strong two-photon absorptions observed in these solids, although detrimental to laser action, are fascinating since they lead to highly excited charge transfer states which are poorly understood. F/Xe/Kr solids, provide a good system for probing these states.

ACKNOWLEDGMENTS

This research was supported by a grant from the National Science Foundation, Grant No. ECS-8914321, and a contract from US Air Force Astronautics Laboratory, Contract No. S04611-90-K-0035. A grant from the Academy of Finland to H. Kunttu during his stay at Irvine is gratefully acknowledged.

[1] N. Schwentner and V. A. Apkarian, Chem. Phys. Lett. **154**, 413 (1989).
[2] A. I. Katz, J. Feld, and V. A. Apkarian, Optics Lett. **14**, 441 (1989).
[3] H. Kunttu, W. G. Lawrence, and V. A. Apkarian, J. Chem. Phys. **94**, 1692 (1991).
[4] M. E. Fajardo and V. A. Apkarian, J. Chem. Phys. **89**, 4124 (1988).
[5] R. K. Steunenberg and R. C. Vogel, J. Am. Chem. Soc. **78**, 901 (1956).
[6] R. Alimi, R. B. Gerber, and V. A. Apkarian, J. Chem. Phys. **92**, 3551 (1990).
[7] H. Kunttu, J. Feld, R. Alimi, A. Becker, and V. A. Apkarian, J. Chem. Phys. **92**, 4856 (1990).
[8] J. Feld, H. Kunttu, and V. A. Apkarian, J. Chem. Phys. **93**, 1009 (1990).
[9] H. Kunttu and V. A. Apkarian, Chem. Phys. Lett. **171**, 423 (1990).
[10] M. E. Fajardo and V. A. Apkarian, J. Chem. Phys. **89**, 4102 (1988).
[11] H. Kunz, J. McCaffery, M. Chergui, R. Schriever, O. Unal, V. Stepanenko, and N. Schwentner, Phys. Rev. B. (submitted).
[12] N. Schwentner, M. E. Fajardo, and V. A. Apkarian, Chem. Phys. Lett. **154**, 237 (1989).
[13] V. A. Apkarian, *Proceedings of the International Conference on Lasers '89*, edited by D. G. Harris and T. M. Shay (STS Press, McLean, VA, 1990), pp. 121–126.
[14] B. S. Ault and L. Andrews, J. Chem. Phys. **65**, 4192 (1976).
[15] J. Goodman and L. E. Brus, J. Chem. Phys. **65**, 3808 (1976).
[16] M. E. Fajardo, R. Withnall, J. Feld, F. Okada, W. Lawrence, L. Wiedeman, and V. A. Apkarian, Laser Chem. **9**, 1 (1988).
[17] J. Le Calve and P. Gurtler, J. Chem. Phys. (Paris) **86**, 1849 (1989).
[18] W. Rudnick, R. Haensel, H. Nahme, and N. Schwentner, Phys. Stat. Solidi A **87**, 319 (1985).
[19] V. Aquilanti, E. Luzzatti, F. Pirani, and G. Volpi, J. Chem. Phys. **89**, 6165 (1988).
[20] C. H. Becker, P. Casavecchia, and Y. T. Lee, J. Chem. Phys. **69**, 2377 (1978); **70**, 2986 (1979).
[21] H. Helm, D. L. Huestis, M. J. Dyer, and D. C. Lorents, J. Chem. Phys. **79**, 3220 (1983).
[22] C. Y. Ng, P. W. Tiedemann, B. H. Mahan, and Y. T. Lee, J. Chem. Phys. **66**, 5737 (1977).
[23] R. E. Behringer, J. Chem. Phys. **29**, 537 (1958).
[24] R. Alimi, R. B. Gerber, and V. A. Apkarian, J. Chem. Phys. **89**, 174 (1988).
[25] R. Alimi, A. Brokman, and R. B. Gerber, J. Chem. Phys. **91**, 1611 (1989).
[26] H. Jara, H. Pummer, H. Egger, and C. K. Rhodes, Phys. Rev. B **30**, 1 (1984).
[27] *Excimer Lasers*, edited by C. K. Rhodes, Topics in Applied Physics (Springer, New York, 1984), Vol. 30.
[28] P. C. Tellinghuisen, J. Tellinghuisen, J. A. Coxon, J. E. Velazco, and D. W. Setser, J. Chem. Phys. **68**, 5187 (1978).
[29] J. Feld, thesis, University of California, Irvine, 1990.
[30] M. E. Fajardo and V. A. Apkarian, J. Chem. Phys. **85**, 5660 (1986).
[31] T. H. Dunning, Jr. and P. J. Hay, J. Chem. Phys. **69**, 134 (1978).
[32] H. C. Brashears, Jr., D. W. Setser, and Y.-C. Yu, J. Chem. Phys. **74**, 10 (1981).
[33] P. Gurtler, H. Kunz, and J. Le Calve, J. Lumin. **40&41**, 237 (1988).
[34] D. C. Lorents, D. L. Huestis, M. V. McCusker, H. H. Nakamo, and R. M. Hill, J. Chem. Phys. **68**, 4657 (1978).
[35] Y. C. Yu and D. W. Setser, J. Phys. Chem. **94**, 2934 (1990).
[36] G. C. Maitland, M. Rigby, E. B. Smith, and W. A. Wakeham, *Intermolecular Forces* (Clarendon, Oxford, 1978), see Appendix 10.
[37] P. M. Dehmer and J. L. Dehmer, J. Chem. Phys. **68**, 3462 (1978).
[38] P. M. Dehmer and J. L. Dehmer, J. Chem. Phys. **69**, 125 (1978).
[39] P. M. Dehmer and S. T. Pratt, J. Chem. Phys. **77**, 4804 (1982).
[40] D. B. Geohegan and J. G. Eden, J. Chem. Phys. **89**, 3410 (1988); A. W. McCown, *ibid.* **94**, 8913 (1990).
[41] I. Last and T. F. George, J. Chem. Phys. **93**, 8925 (1990), and references therein.